Biomedical Optics EXPRESS

In vivo imaging of immune cell dynamics in skin in response to zinc-oxide nanoparticle exposure

Benedikt W. Graf,[1,2] Eric J. Chaney,[1] Marina Marjanovic,[1] Michael De Lisio,[1,3] Maria C. Valero,[1] Marni D. Boppart,[1,3] and Stephen A. Boppart[1,2,4,*]

[1]*Beckman Institute for Advanced Science and Technology Beckman Institute for Advanced Science and Technology University of Illinois at Urbana-Champaign, Urbana, IL USA*
[2] *Department of Electrical and Computer Engineering University of Illinois at Urbana-Champaign, Urbana, IL USA*
[3]*Department of Kinesiology and Community Health University of Illinois at Urbana-Champaign, Urbana, IL USA*
[4]*Departments of Bioengineering and Internal Medicine University of Illinois at Urbana-Champaign, Urbana, IL USA*
[*]*boppart@illinois.edu*

Abstract: Zinc oxide (ZnO) nanoparticles (NPs) are widely used in cosmetic and sunscreen products which are applied topically to the skin. Despite their widespread use, the safety and biological response of these particles remains an active area of investigation. In this paper we present methods based on *in vivo* multiphoton microscopy (MPM) in skin to address relevant questions about the potential toxicity and immunological response of ZnO NPs. Registration of time-lapse volumetric MPM images allows the same skin site to be tracked across multiple days for visualizing and quantifying cellular and structural changes in response to NP exposure. Making use of the unique optical properties of ZnO enables high contrast detection of the NPs in the presence of strong autofluorescence and second harmonic generation (SHG) background from the skin. A green fluorescent protein (GFP) bone marrow (BM) transplanted mouse model is used to visualize and assess the dynamic response of BM-derived immune cells. These cells are visualized to assess the potential for ZnO NPs to interact with immune cells and elicit an immune reaction in skin. We investigate both topical and dermal exposure of the ZnO NPs. The methods and findings presented in this paper demonstrate a novel approach for tracking ZnO NPs *in vivo* and for visualizing the cellular response of the exposed tissue to assess the immunological response and potential toxicity of these particles.

©2013 Optical Society of America

OCIS codes: (180.4315) Nonlinear microscopy; (170.0170) Medical optics and biotechnology; (160.4236) Nanomaterials; (170.1420) Biology.

References and links

1. M. D. Newman, M. Stotland, and J. I. Ellis, "The safety of nanosized particles in titanium dioxide- and zinc oxide-based sunscreens," J. Am. Acad. Dermatol. **61**(4), 685–692 (2009).
2. H. Hidaka, H. Kobayashi, T. Koike, T. Sato, and N. Serpone, "DNA damage photoinduced by cosmetic pigments and sunscreen agents under solar exposure and artificial UV illumination," J. Oleo Sci. **55**(5), 249–261 (2006).
3. H. A. Jeng and J. Swanson, "Toxicity of metal oxide nanoparticles in mammalian cells," J. Environ. Sci. Health Part A-Toxic/Hazard. Subst. Environ. Eng. **41**(12), 2699–2711 (2006).
4. S. E. Cross, B. Innes, M. S. Roberts, T. Tsuzuki, T. A. Robertson, and P. McCormick, "Human skin penetration of sunscreen nanoparticles: *In-vitro* assessment of a novel micronized zinc oxide formulation," Skin Pharmacol. Physiol. **20**(3), 148–154 (2007).
5. A. O. Gamer, E. Leibold, and B. van Ravenzwaay, "The *in vitro* absorption of microfine zinc oxide and titanium dioxide through porcine skin," Toxicol. In Vitro **20**(3), 301–307 (2006).
6. E. Gontier, C. Habchi, T. Pouthier, P. Aguer, P. Barberet, Y. Barbotteau, S. Incerti, M. D. Ynsa, J. E. Surleve-Bazeille, and P. Moretto, "Nuclear microscopy and electron microscopy studies of percutaneous penetration of nanoparticles in mammalian skin," J. Invest. Dermatol. **123**, (2004).
7. B. Gulson, M. McCall, M. Korsch, L. Gomez, P. Casey, Y. Oytam, A. Taylor, M. McCulloch, J. Trotter, L. Kinsley, and G. Greenoak, "Small amounts of zinc from zinc oxide particles in sunscreens applied outdoors are absorbed through human skin," Toxicol. Sci. **118**(1), 140–149 (2010).

#192235 - $15.00 USD Received 14 Jun 2013; revised 9 Aug 2013; accepted 11 Aug 2013; published 29 Aug 2013

8. L. W. Zhang and N. A. Monteiro-Riviere, "Assessment of quantum dot penetration into intact, tape-stripped, abraded and flexed rat skin," Skin Pharmacol. Physiol. **21**(3), 166–180 (2008).
9. J. G. Rouse, J. Z. Yang, J. P. Ryman-Rasmussen, A. R. Barron, and N. A. Monteiro-Riviere, "Effects of mechanical flexion on the penetration of fullerene amino acid-derivatized peptide nanoparticles through skin," Nano Lett. **7**(1), 155–160 (2007).
10. M. Crosera, M. Bovenzi, G. Maina, G. Adami, C. Zanette, C. Florio, and F. Filon Larese, "Nanoparticle dermal absorption and toxicity: a review of the literature," Int. Arch. Occup. Environ. Health **82**(9), 1043–1055 (2009).
11. S. Kim, Y. T. Lim, E. G. Soltesz, A. M. De Grand, J. Lee, A. Nakayama, J. A. Parker, T. Mihaljevic, R. G. Laurence, D. M. Dor, L. H. Cohn, M. G. Bawendi, and J. V. Frangioni, "Near-infrared fluorescent type II quantum dots for sentinel lymph node mapping," Nat. Biotechnol. **22**(1), 93–97 (2004).
12. N. V. Gopee, D. W. Roberts, P. Webb, C. R. Cozart, P. H. Siitonen, A. R. Warbritton, W. W. Yu, V. L. Colvin, N. J. Walker, and P. C. Howard, "Migration of intradermally injected quantum dots to sentinel organs in mice," Toxicol. Sci. **98**(1), 249–257 (2007).
13. C. Hanley, A. Thurber, C. Hanna, A. Punnoose, J. Zhang, and D. G. Wingett, "The influences of cell type and ZnO nanoparticle size on immune cell cytotoxicity and cytokine induction," Nanoscale Res. Lett. **4**(12), 1409–1420 (2009).
14. J. Schulz, H. Hohenberg, F. Pflücker, E. Gärtner, T. Will, S. Pfeiffer, R. Wepf, V. Wendel, H. Gers-Barlag, and K. P. Wittern, "Distribution of sunscreens on skin," Adv. Drug Deliv. Rev. **54**(Suppl 1), S157–S163 (2002).
15. NANODERM, "Quality of skin as a barrier to ultra-fine particles. final report.," Project Number: QLK4-CT-2002–02678 (2007).
16. J. Lademann, H. J. Weigmann, C. Rickmeyer, H. Barthelmes, H. Schaefer, G. Mueller, and W. Sterry, "Penetration of titanium dioxide microparticles in a sunscreen formulation into the horny layer and the follicular orifice," Skin Pharmacol. Appl. Skin Physiol. **12**(5), 247–256 (1999).
17. A. Mavon, C. Miquel, O. Lejeune, B. Payre, and P. Moretto, "*In vitro* percutaneous absorption and *in vivo* stratum corneum distribution of an organic and a mineral sunscreen," Skin Pharmacol. Physiol. **20**(1), 10–20 (2007).
18. W. Denk, J. H. Strickler, and W. W. Webb, "Two-photon laser scanning fluorescence microscopy," Science **248**(4951), 73–76 (1990).
19. B. R. Masters, P. T. C. So, and E. Gratton, "Multiphoton excitation fluorescence microscopy and spectroscopy of *in vivo* human skin," Biophys. J. **72**(6), 2405–2412 (1997).
20. K. Koenig and I. Riemann, "High-resolution multiphoton tomography of human skin with subcellular spatial resolution and picosecond time resolution," J. Biomed. Opt. **8**(3), 432–439 (2003).
21. B. W. Graf and S. A. Boppart, "Multimodal *in vivo* skin imaging with integrated optical coherence and multiphoton microscopy," IEEE J. Sel. Top. Quantum Electron. **18**(4), 1280–1286 (2012).
22. K. König, "Clinical multiphoton tomography," J. Biophotonics **1**(1), 13–23 (2008).
23. B. W. Graf, M. C. Valero, E. J. Chaney, M. Marjanovic, M. D. Boppart, and S. A. Boppart, "Long-term time-lapse multimodal microscopy for tracking cell dynamics in live tissue," Proc. SPIE **7902**, 790206 (2011).
24. S. K. Das, M. Biswas, D. Byrne, M. Bock, E. McGlynn, M. Breusing, and R. Grunwald, "Multiphoton-absorption induced ultraviolet luminescence of ZnO nanorods using low-energy femtosecond pulses," J. Appl. Phys. **108**(4), 043107 (2010).
25. D. C. Dai, S. J. Xu, S. L. Shi, M. H. Xie, and C. M. Che, "Efficient multiphoton-absorption-induced luminescence in single-crystalline ZnO at room temperature," Opt. Lett. **30**(24), 3377–3379 (2005).
26. A. V. Zvyagin, X. Zhao, A. Gierden, W. Sanchez, J. A. Ross, and M. S. Roberts, "Imaging of zinc oxide nanoparticle penetration in human skin *in vitro* and *in vivo*," J. Biomed. Opt. **13**(6), 064031 (2008).
27. M. S. Roberts, M. J. Roberts, T. A. Robertson, W. Sanchez, C. Thörling, Y. H. Zou, X. Zhao, W. Becker, and A. V. Zvyagin, "*In vitro* and *in vivo* imaging of xenobiotic transport in human skin and in the rat liver," J Biophotonics **1**(6), 478–493 (2008).
28. Z. Song, T. A. Kelf, W. H. Sanchez, M. S. Roberts, J. Rička, M. Frenz, and A. V. Zvyagin, "Characterization of optical properties of ZnO nanoparticles for quantitative imaging of transdermal transport," Biomed. Opt. Express **2**(12), 3321–3333 (2011).
29. L. L. Lin, J. E. Grice, M. K. Butler, A. V. Zvyagin, W. Becker, T. A. Robertson, H. P. Soyer, M. S. Roberts, and T. W. Prow, "Time-correlated single photon counting for simultaneous monitoring of zinc oxide nanoparticles and NAD(P)H in intact and barrier-disrupted volunteer skin," Pharm. Res. **28**(11), 2920–2930 (2011).
30. B. W. Graf, E. J. Chaney, M. Marjanovic, S. G. Adie, M. De Lisio, M. C. Valero, M. D. Boppart, and S. A. Boppart, "Long-term time-lapse multimodal intravital imaging of regeneration and bone-marrow-derived cell dynamics in skin," Technology. In Press.
31. R. P. Kataru, K. Jung, C. Jang, H. Yang, R. A. Schwendener, J. E. Baik, S. H. Han, K. Alitalo, and G. Y. Koh, "Critical role of CD11b(+) macrophages and VEGF in inflammatory lymphangiogenesis, antigen clearance, and inflammation resolution," Blood **113**(22), 5650–5659 (2009).
32. J. J. Jones, I. D. McGilvray, A. B. Nathens, R. Bitar, and O. D. Rotstein, "Glutathione depletion prevents lipopolysaccharide-induced local skin inflammation," Arch. Surg. **132**(11), 1165–1169, discussion 1170 (1997).
33. H. G. Breunig, H. Studier, and K. König, "Multiphoton excitation characteristics of cellular fluorophores of human skin *in vivo*," Opt. Express **18**(8), 7857–7871 (2010).

#192235 - $15.00 USD Received 14 Jun 2013; revised 9 Aug 2013; accepted 11 Aug 2013; published 29 Aug 2013
(C) 2013 OSA

1. Introduction

The use of nanoparticles (NPs) in consumer products such as cosmetics and sunscreens has become common in recent decades. Despite their widespread use, concerns about the safety of these materials remain [1]. One type of NP that is commonly used as a sun blocking agent is zinc-oxide (ZnO). Nanosized ZnO is an efficient absorber in the ultraviolet (UV) spectral region yet is transparent in the visible spectrum, making it attractive for use in cosmetics and sunscreens. The primary safety concern regarding ZnO NPs is their potential for generating free radicals in response to UV illumination, which can result in DNA damage in cells and an immunological response [2, 3]. Despite this potential toxicity, ZnO NPs are generally considered to be safe for use in topically-applied skin products as long as they are not absorbed through the skin or pass through breaches in the protective skin barrier. Thus, a primary focus in evaluating the safety of ZnO NPs has been assessing their ability to penetrate skin.

Several studies have demonstrated that ZnO nanoparticles generally do not penetrate past the stratum corneum [4–6], the outer-most layer of the skin. However, a recent *in vivo* study based on a sensitive radiolabeling technique detected small amounts of ZnO penetration [7]. In addition, there is concern that NP absorption could be enhanced in situations where the barrier function of the skin is reduced, either by injury or disease [1, 8]. It has also been demonstrated that mechanical flexing of skin during NP exposure can result in penetration into the dermis [9]. As a result, characterizing the potential for ZnO NP penetration through skin remains an active area of investigation. As studies have demonstrated that NP penetration through skin is possible under certain conditions, there is also an interest in understanding the consequences of skin penetration by NPs, such as an immunological response. The biodistribution and long-term fate of ZnO NPs that have penetrated the skin is fundamentally important for assessing the biological response of their presence and ultimately, their toxicity. Studies of other types of NPs in skin have demonstrated that intradermally-administered particles migrate to regional lymph nodes, raising concerns about their potential for affecting the immune system [10–12]. In addition, the toxicity of ZnO NPs to human immune cells has been established in *in vitro* studies [13], leading to concerns about immune toxicity. Given the remaining concerns about the safety of ZnO NPs, there is a critical need for novel methods for assessing their spatiotemporal dynamics over extended periods of time, and the different factors that can affect their toxicity.

Various methods have been applied for studying NP penetration in skin. Several studies have utilized diffusion chambers to study the penetration of ZnO NPs through *in vitro* skin samples [4, 5]. Other studies have been based on the application of NPs to the skin, either *in vivo* or *in vitro*, for a fixed time period followed by analysis of the tissue. Penetration depth of NPs can then be assessed by histological processing of skin followed by optical or electron microscopy [14, 15]. An alternative technique, known as the tape stripping method, has routinely been used, whereby the skin layers are removed sequentially starting at the surface [16, 17]. While these methods are suitable for assessing the penetration of NPs at fixed time points, they are limited in that they require destruction of the tissue samples. This precludes the ability to track the time-dependent penetration of the NPs or study dynamic cellular or structural changes of the tissue in response to the NP exposure. In addition, histological processing of the tissue may introduce artifacts and the tape stripping method is inherently not suitable for visualizing the spatial locations of NPs in the skin.

A promising technique that has been recently applied for studying the penetration of ZnO NPs is multiphoton microscopy (MPM) [18]. MPM is an imaging technique that makes use of nonlinear optical effects to generate high resolution images. MPM is well-suited for non-invasively imaging intact tissue such as skin [19–21]. Primary applications of skin imaging include visualizing cellular features for clinical applications [22] or study cellular dynamics *in vivo* [23]. Imaging studies of ZnO NP penetration in skin take advantage of the unique optical properties exhibited by ZnO. Multiphoton excitation of ZnO results in a narrowband two-photon luminescence signal centered around 395 nm, a broadband signal centered around

#192235 - $15.00 USD Received 14 Jun 2013; revised 9 Aug 2013; accepted 11 Aug 2013; published 29 Aug 2013
(C) 2013 OSA

490 nm, and a second harmonic generation (SHG) signal [24, 25]. The ability to noninvasively visualize high resolution features of intact skin as well as the spatiotemporal distributions of ZnO makes MPM an attractive method for tracking the penetration of ZnO NPs in skin. Such studies have been performed in human skin *in vivo* and have confirmed that ZnO NPs do not penetrate the stratum corneum in intact skin, although they can accumulate in hair follicles [26, 27]. One challenge of using MPM for ZnO toxicity studies is the difficulty of separating the ZnO optical signals from autofluorescence or SHG due to collagen in the skin [28, 29]. In addition, despite the successful application of MPM for assessing the penetration of ZnO nanoparticles in skin, the potential of this technique has yet to be fully exploited. The noninvasive nature of MPM potentially enables time-lapse imaging of exposed skin to observe the time-dependent transport of ZnO NPs, in addition to observing the dynamic biological response of the skin. In this paper, we also demonstrate methods and results for time-lapse tracking of ZnO NPs in the same skin site and for visualizing the response of immune cells to the presence of these NPs in the dermis. These methods are based on registration of time-lapse, wide-area, volumetric MPM images of the skin of green fluorescent protein (GFP) bone marrow (BM) transplanted mice. In these mice, immune cells derived from the BM express GFP and can be imaged with two-photon-excited fluorescence (TPEF), providing an opportunity to visualize immune responses to the presence of foreign compounds or nanoparticles. These methods represent novel capabilities for assessing the safety of ZnO nanoparticles that are used in commercial cosmetic and sunscreen products.

2. Method

2.1 In vivo MPM skin imaging

For this study, a custom-built multiphoton microscope based on a tunable Ti-Sapphire laser (Mai Tai HP, Spectra Physics) was utilized [21]. The laser beam was sent though a pair of scanning mirrors, a 3.5x beam-expanding telescope, and was focused onto the sample with a 0.95 numerical aperture (NA) objective (XLUMP20X, Olympus). Two-photon luminescence signal (TPL), two-photon excited fluorescence (TPEF), and second harmonic generation (SHG) signals were collected by the objective and diverted to a pair of photo-multiplier tubes (PMTs) using a dichroic mirror. An additional low pass dichroic mirror split the signal into two separate channels, each containing a lens, an appropriate emission filter, and a PMT. Samples were positioned on a motorized stage which allowed depth focusing and the acquisition of wide-area mosaics. Individual MPM images were acquired in ~1.5 seconds and the field-of-view of was ~370 x 370 μm^2. *In vivo* imaging in mouse skin was performed by anesthetizing the mice with isoflurane gas. Mice were placed on a heating pad mounted to the motorized stage of the microscope. The ear skin was positioned against a coverslip following the application of glycerol for index matching. The skin was held in place by applying slight pressure with a gauze covered clamp. MPM imaging was performed at two different excitation wavelengths, 720 nm for efficient excitation of ZnO TPL and 920 nm for TPEF imaging of GFP cells, in addition to SHG from collagen and ZnO NPs. Power at the sample at 720 nm and 920 nm was 3 mW and 20 mW, respectively. TPEF images from the skin contain significant levels of autofluorescence background, primarily from hair shafts. As the TPEF signal from the GFP cells is used as a relative measure of the presence of BM-derived cells, it is important to remove strong autofluorescent features. To remove these features, a segmentation technique was implemented that extracts the hair shaft features from volumetric images based on their size and aspect ratio [30]. The segmentation technique relies on the fact that hair shafts are spatially separated from the GFP-expressing cells located in the skin. This is a valid assumption as hair shafts reside on the surface of the skin or within hair follicles. Once the hair shafts are segmented they are digitally subtracted from the image volumes.

2.2 Registration of time-lapse images

Volumetric MPM images were acquired at different time points at the same skin locations on the mouse ear. Bulk alignment was accomplished by using blood vessels as landmarks. In

#192235 - $15.00 USD Received 14 Jun 2013; revised 9 Aug 2013; accepted 11 Aug 2013; published 29 Aug 2013
(C) 2013 OSA

order to accurately align the time-lapse images and quantify changes, a registration algorithm was developed [30]. This algorithm makes use of the hair follicle positions in the SHG images as landmarks for the registration in the two lateral dimensions. The first step of the algorithm is a semi-automated identification of the hair follicle positions in the wide-area SHG mosaics from the two time points. Next, matching of the follicles is automatically performed by exploiting the diversity in the spatial patterns. The matching follicle positions are used to define a transformation between the two time points that is represented by the thin-plate spline function. This transformation function is then used to warp all the images from one time point so that the multimodal time-lapse images are co-registered.

2.3 GFP BM-transplanted mice

GFP BM-transplanted mice were used in this study to enable visualization of the BM-derived immune cells in the skin. These mice were created by transplanting BM from donor males with constitutive GFP expression (C57BL/6-Tg (CAG-EGFP) 10sb/J) into wild-type recipients. To harvest BM, mice were sacrificed via CO_2 inhalation, hind limb bones were dissected, cleaned, placed in phosphate buffered solution (PBS), and crushed with a mortar and pestle. The crushed solution was strained with a 40 micron filter and red blood cells were lysed with an ACK lysing buffer. Cell concentration was counted and diluted to approximately $7x10^6$ cells/ml and kept on ice prior to transplant. Recipient female C57BL/6 wild-type mice were treated with radiation from a cobalt-60 source (2 doses of 6 GY, administered 4 hours apart). Donor bone-marrow cells were transplanted by tail vein injection (150 μl, 10^6 cells). Recipient mice were allowed to recover for 4 weeks prior to confirming the successful engraftment by detecting GFP expressing cells in the skin by *in vivo* MPM imaging. Experiments were performed in compliance with an experimental protocol approved by the institutional animal care and use committee at the University of Illinois at Urbana-Champaign.

2.4 Zinc oxide nanoparticle exposure

The ZnO NPs used in this study were uncoated particles with an average diameter of ~35 nm suspended in an aqueous solution at a concentration of 50 wt% (721077, Sigma). This solution was applied both topically and intradermally to the mouse skin. For topical application, the skin was exposed to the solution for one hour followed by rinsing with water to remove excess particles. For intradermal exposure, ~0.5 mm long linear incisions were made in the mouse ear skin using a surgical blade under the guidance of a stereo microscope. Incisions were exposed to either the ZnO NP solution or a control water treatment for one hour and then rinsed with water. As a positive control for detecting the immune response of the BM-derived GFP cells, lipopolysaccharide (LPS) was applied to linear incisions in the ear skin (500 μg in 50 μl phosphate buffered saline).

3. Results

3.1 In vivo imaging of BM-derived immune cells

In vivo MPM imaging of GFP BM transplanted mouse ear skin was performed under normal conditions to demonstrate the ability to visualize BM-derived cells (Fig. 1). Three-dimensional renderings of the volumetric SHG images provide a high resolution view of the collagen network in the dermis (Fig. 1(a)) while TPEF images enable individual BM-derived cells to be resolved (Fig. 1(b)). Wide-area volumetric images were acquired by using a motorized stage, providing a macroscopic view of the skin structure and the BM-derived cell population. The volumetric images are represented as axial projections by summing the pixel intensities along the depth dimension (Fig. 1(c)-1(e)). Raw TPEF images contain auto fluorescence background from hair shafts. These features are digitally removed from the volumetric images using a segmentation procedure. Removing the autofluorescence signal is important in order to isolate the fluorescence signal from the GFP cells. The remaining TPEF signal is primarily due to the GFP-expressing cells derived from the BM. Thus, the TPEF

#192235 - $15.00 USD Received 14 Jun 2013; revised 9 Aug 2013; accepted 11 Aug 2013; published 29 Aug 2013
(C) 2013 OSA

images are a representation of the density of BM-derived immune cells present in the skin. As the *in vivo* imaging is non-invasive, repeated imaging of the same skin site is possible. This allows dynamic changes in BM-derived cell population to be tracked in response to exposure to foreign compounds.

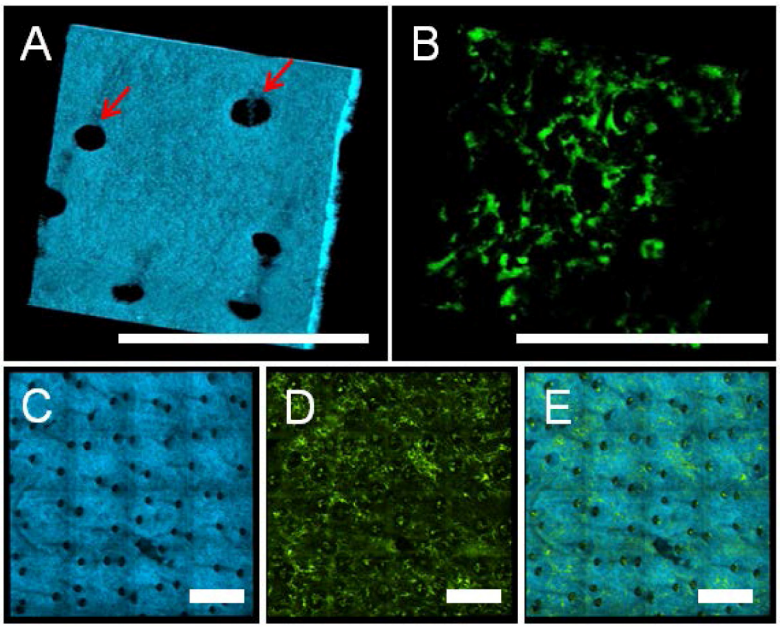

Fig. 1. *In vivo* MPM imaging of GFP bone marrow transplanted mouse skin. High resolution renderings of (A) SHG and (B) TPEF image volumes. SHG images visualize the collagen network in the dermis and TPEF images show individual BM-derived cells. Dark circular features in the SHG images indicated by red arrows are hair follicles. Wide area mosaics of the skin based on (C) SHG, (D) TPEF and (E) multimodal overlays to show spatial correspondence. *In vivo* imaging allows the density of BM-derived cells and spatial positions within the skin to be non-invasively assessed. The BM derived cells in the skin are a heterogeneous population including several different types of immune cells, including macrophages, neutrophils, and dendritic cells. Scale bars are 300 μm.

3.2 In vivo imaging of an immune response to a known inflammatory agent

To demonstrate the ability to visualize an immune response by BM-derived GFP cells and to serve as a positive control for this study, *in vivo* imaging was performed in the ear skin after dermal exposure to lipopolysaccharide (LPS). LPS is a known inflammatory agent which has been used to induce immune reactions in skin [31, 32]. Volumetric wide-area TPEF and SHG images were acquired prior to the treatment to determine the relative density of GFP cells in the steady state (Fig. 2(a), 2(c), 2(e)). A linear incision was made in the skin to expose the dermal layer and the LPS solution was applied for one hour. *In vivo* imaging 24 hours post-exposure demonstrated a dramatic increase in the GFP signal in the skin as well as the structural changes resulting from the incision (Fig. 2(b), 2(d), 2(f)). The images in Fig. 2(a)-2(f) are displayed on the same intensity scale to demonstrate the significant increase in the level of the GFP signal following the treatment. In order to visualize the cellular features of the GFP signal, the intensity scaling of the GFP channel is adjusted in the GFP-SHG overlay following the treatment (Fig. 2(g)). A high magnification view of the wound site demonstrates that the increased GFP signal consists of many individual GFP cells (Fig. 2(h)). This rapid and dramatic increase of BM-derived cells is expected during inflammation. Thus, the *in vivo* imaging provides a means for non-invasively imaging the inflammatory response and dynamics of the BM-derived cells.

#192235 - $15.00 USD Received 14 Jun 2013; revised 9 Aug 2013; accepted 11 Aug 2013; published 29 Aug 2013
(C) 2013 OSA

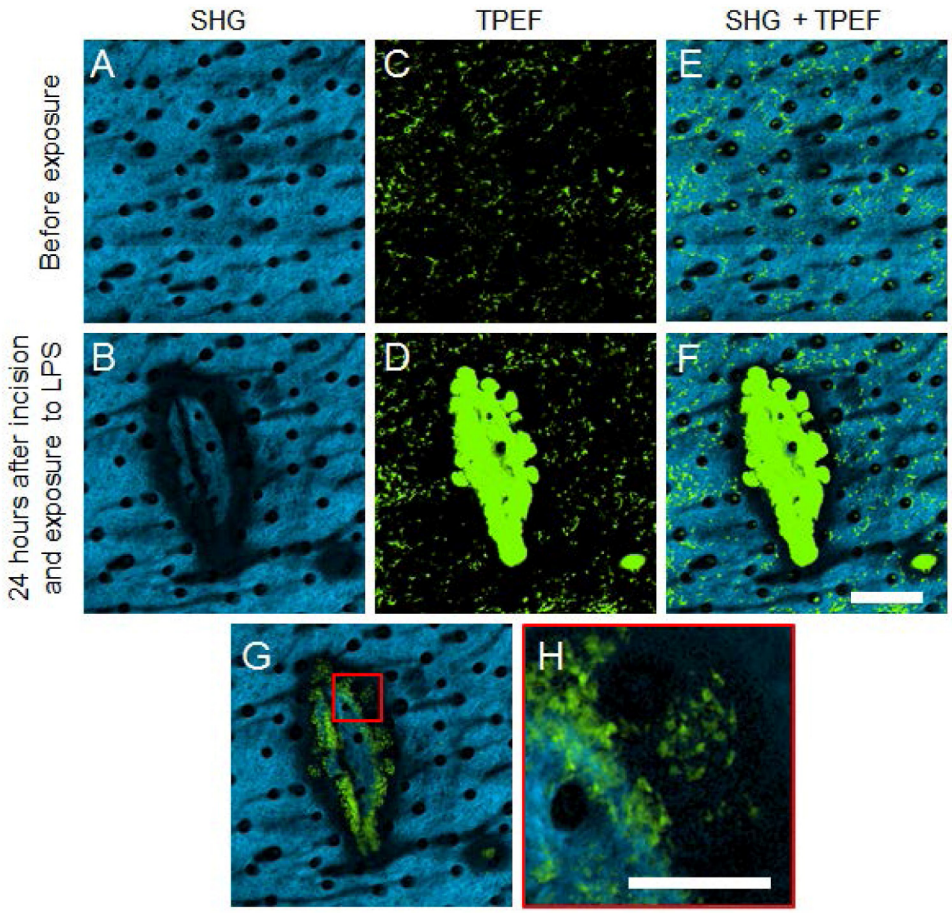

Fig. 2. *In vivo* imaging of BM-derived GFP cell dynamics in skin during an immune reaction. (A, B) SHG, (C, D) TPEF and (E, F) overlaid *en face* sections of *in vivo* mouse skin (A, C, E) before and (B, D, F) 24 hours after a linear incision and exposure to lipopolysaccharide (LPS). Intensity scaling of the GFP images in (C) and (D) are the same in order to demonstrate the large increase in GFP signal. (G) Overlaid *en face* section 24 hours after the wound with the intensity scale of the GFP image adjusted to allow the cellular features of the GFP signal to be seen. (H) A higher magnification *en face* section of the region marked by the red box in (G) showing individual GFP cells. Scale bar for (A-G) is 300 μm and 100 μm for (H).

3.3 Imaging ZnO NPs in skin

MPM is a promising technique for visualizing the penetration and long-term fate of ZnO NPs that are applied to the skin. However, a primary challenge is separating the optical signal from ZnO from the autofluorescence and SHG background from skin. To facilitate the discrimination of ZnO NPs from background we make use of both the TPL and SHG signals that result from two-photon excitation. Figure 3 shows *in vivo* imaging of linear incisions in mouse skin with and without exposure to ZnO NPs. SHG signal originates both from the collagen in the dermis as well as the ZnO NPs (Fig. 3(a) and 3(b)). SHG imaging is performed at an excitation wavelength of 920 nm with an emission filter centered at 447 nm. This specific excitation wavelength was chosen because it provides optimal excitation of GFP and also results in a lower TPL signal from ZnO. TPL signal originates from the ZnO NPs as well from autofluorescent features within the skin (Fig. 3(c) and 3(d)). TPL imaging is performed at 720 nm with an emission filter centered at 390 nm. This excitation wavelength provides a strong TPL signal from the ZnO particles but a low SHG signal. As ZnO generates

#192235 - $15.00 USD Received 14 Jun 2013; revised 9 Aug 2013; accepted 11 Aug 2013; published 29 Aug 2013
(C) 2013 OSA

both TPL and SHG [24], the TPL and SHG channels are merged by multiplying pixel intensities. This provides enhanced contrast of the ZnO NPs and suppresses the autofluorescence and SHG from collagen. This approach generally assumes that background autofluorescence and SHG do not originate from the same features in the skin. This is a valid approximation as SHG comes from collagen in the dermis while autofluorescence is strongest in the upper layers of the skin such as the stratum corneum, in addition to the hair shafts [33]. As seen in Fig. 3(e) and 3(f), the merging of the channels provides enhancement of the ZnO signal and suppression of the background signal.

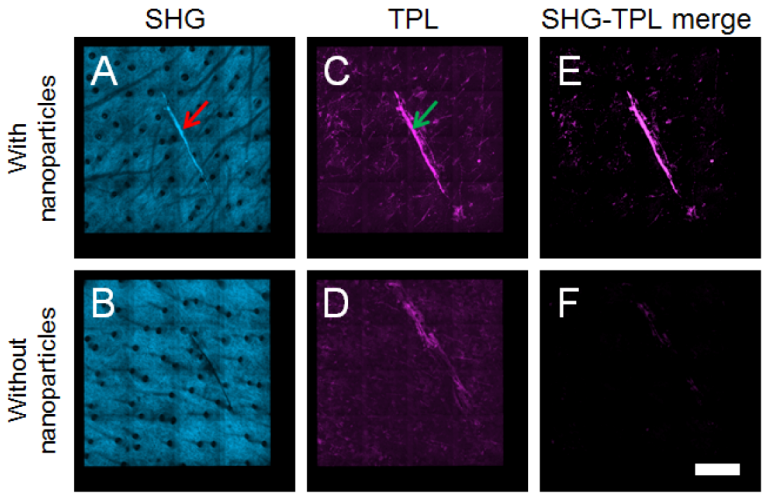

Fig. 3. Imaging zinc-oxide (ZnO) nanoparticles in the presence of skin auto-fluorescence based on SHG and TPL. (A, B) SHG channel, (C, D) TPL channel and (E, F) merged channels from *in vivo* mouse skin images following a linear incision and (A, C, E) ZnO particle exposure or (B, D, F) a control without particles. ZnO particles generate both SHG (red arrow) and TPL (green arrow) and thus merging the two channels discriminates ZnO particles from the autofluorescence background which only appears in the TPL channel. Scale bar is 300 μm.

3.4 In vivo imaging of topical ZnO NP exposure

In order to evaluate the potential for ZnO NPs to interact with the BM-derived immune cells and cause an inflammatory response, time-lapse imaging was performed in GFP BM-transplanted mouse skin following topical exposure to ZnO NPs. Volumetric SHG/TPEF and TPL data sets were acquired at four different time points: prior to the exposure, immediately after exposure, and 24 and 48 hours after exposure (Fig. 4). The exposure consisted of a one-hour topical application of an aqueous ZnO solution (50 wt%) to a region of skin marked by tape followed by rinsing with water. The merged images of the ZnO NPs demonstrate a dramatic rise in signal following exposure and a gradual decrease over the 48 hour post-exposure time period.

3.5 In vivo imaging of dermal ZnO NP exposure

To evaluate the potential response of penetration and dermal exposure of ZnO NPs, time-lapse imaging was performed in GFP BM-transplanted mouse skin following dermal exposure. Dermal exposure was realized by making a linear incision to expose the dermis of the skin, followed by a one-hour treatment of the aqueous ZnO NP solution (50 wt%) or a control solution of water. Volumetric SHG/TPEF and TPL data sets were acquired at four different time points; prior to the exposure, immediately after the exposure, and 24 and 48 hours after the exposure (Fig. 5). The ZnO signal in the case of the dermal exposure (Fig. 5(a)) shows a significant accumulation of the particles within the incision. These particles persist within the wound site for the duration of the imaging sequence. In the control case

#192235 - $15.00 USD Received 14 Jun 2013; revised 9 Aug 2013; accepted 11 Aug 2013; published 29 Aug 2013
(C) 2013 OSA

following an incision (Fig. 5(b)), there is a weak ZnO signal present immediately after the treatment, which is due to autofluorescence.

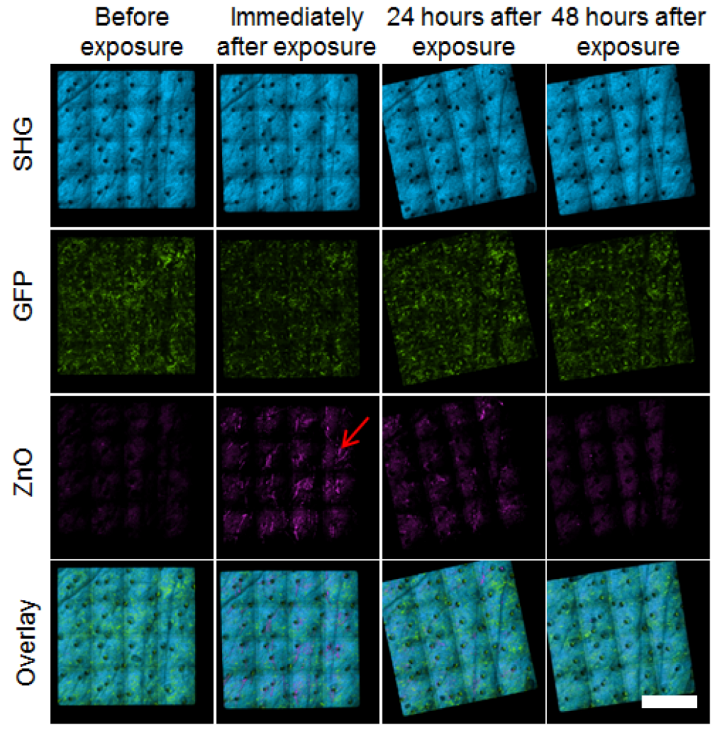

Fig. 4. Time-lapse *in vivo* imaging of mouse skin following topical exposure to ZnO NPs. The MPM signal due to ZnO particles is evident following the exposure (red arrow) and gradually reduces over the 48 hours time period. No significant increase in the GFP signal is observed, indicating no immune response was caused by the presence of the ZnO NPs. Scale bar is 500 µm.

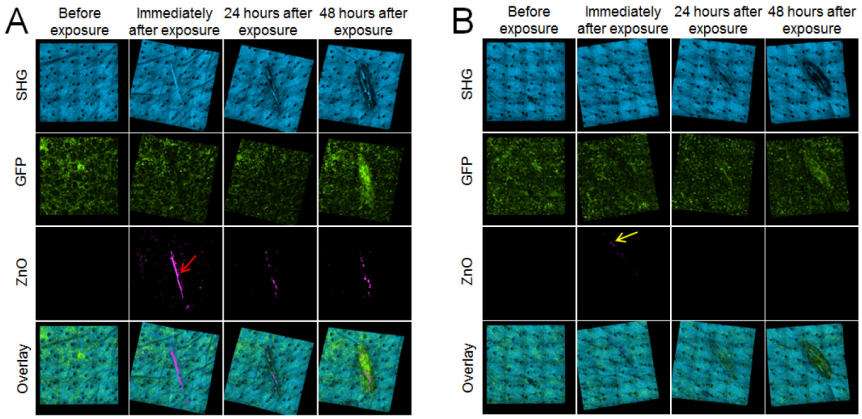

Fig. 5. Time-lapse *in vivo* imaging of mouse skin following a linear incision and dermal exposure to (A) ZnO NPs and (B) a control treatment of water. The accumulation of the ZnO particles in the incision (red arrow) and their persistence over the 48 hour time period is apparent. The ZnO images from the control treatment contains a weak autofluorescence signal (yellow arrow). In both the ZnO exposure and the control, the GFP signal does not significantly increase by 24 hours after the treatment and only slightly increases by 48 hours. This suggests that the exposure to ZnO NPs does not result in a significantly increased inflammatory response compared to the control treatment. Scale bar is 300 µm.

#192235 - $15.00 USD Received 14 Jun 2013; revised 9 Aug 2013; accepted 11 Aug 2013; published 29 Aug 2013
(C) 2013 OSA

In both the control and ZnO NP exposure, no significant increase in the GFP signal was detected by 24 hours post-treatment. There was a slight increase in signal within the wound site by 48 hours. To determine whether this GFP signal was due to an influx of GFP cells or simply the result of strong autofluorescence from the wound site, the increase in the level of GFP signal compared to the LPS exposure positive control treatment was quantified. Figure 6(a) shows the relative change in GFP signal over the 48 hour time period for the LPS, topical ZnO, dermal ZnO, and dermal control treatments. It is apparent that none of the ZnO treatments or the control incision results in a significant increase in the GFP signal when compared to the LPS treatment. In addition, the high resolution images allow cells to be identified based on the morphology. *En face* sections of the GFP channel from the incision sites following the ZnO dermal exposure at 48 hours, the control dermal treatment at 48 hours, and the positive control LPS exposure at 24 hours, are shown in Fig. 6(b)-6(d), respectively. The images from the LPS exposure study contain many cell like features (Fig. 6(d)) while the images from the ZnO treatment do not.

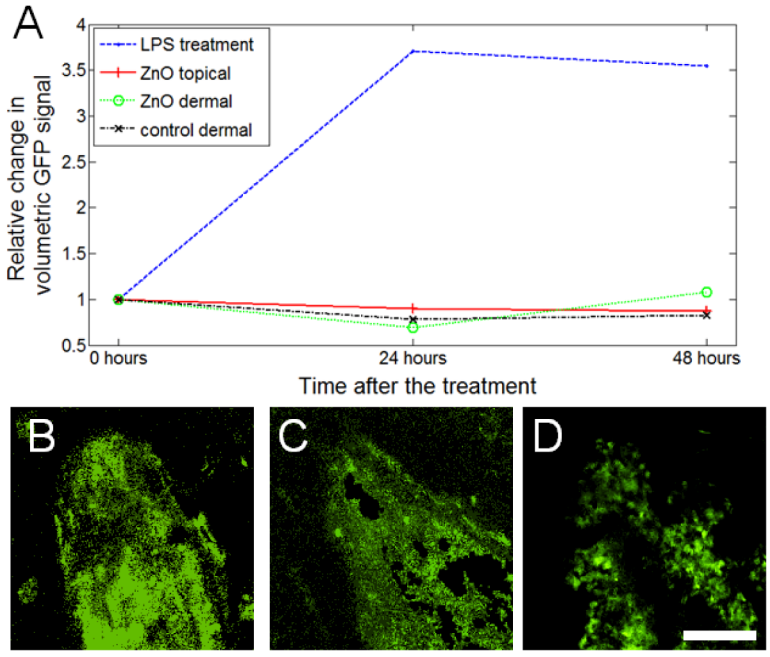

Fig. 6. (A) Quantitative plots of the total GFP signal intensity within the time-lapse image volumes demonstrates that neither topical exposure or dermal exposure of ZnO NPs has elicited a strong immune response. Magnified *en face* sections of the incision sites for (B) ZnO dermal exposure at 48 hours, (C) control dermal treatment at 48 hours and the (D) positive control LPS exposure at 24 hours. The lack of any cellular features in (B) and (C) compared to (D) suggests that this GFP signal is due to a strong autofluorescence from the wound site and not BM-derived GFP cells. Scale bar is 100 μm.

4. Discussion

In this paper, we have demonstrated methods and results for *in vivo* skin imaging to visualize and track ZnO NPs and observe the dynamic response of BM-derived immune cells. TPEF imaging allows GFP cells in the skin to be visualized while SHG signal from collagen provides a view of the structure of the dermis. In order to visualize the dynamic response of immune cells to ZnO NP exposure, GFP BM-transplanted mice were used in this study. In these mice, the BM, and all the nucleated cells derived from the BM, express GFP, and can thus be detected by TPEF imaging. Hematopoietic stem cells in the BM give rise to a wide range of immune cells, including macrophages, neutrophils, dendritic cells, and lymphocytes.

#192235 - $15.00 USD Received 14 Jun 2013; revised 9 Aug 2013; accepted 11 Aug 2013; published 29 Aug 2013
(C) 2013 OSA

Many of these cell types traffic through skin under steady state conditions and increase dramatically in number during injury, inflammation, or immunological responses. The combination of TPEF and SHG allows these BM derived immune cells to be observed within their *in vivo* tissue environment (Fig. 1). This imaging technique has many advantages that can complement standard methods for analyzing tissue based on histology. Most importantly, it allows repeated observation of the BM-derived cells for tracking dynamic behavior.

Using image registration of time-lapse volumetric data sets allows the same skin site to be observed over multiple days. This allows *in vivo* observation of long term dynamic events, such as inflammation. To demonstrate this ability, time-lapse imaging of GFP BM-transplanted mouse skin was performed following dermal exposure to a known inflammatory agent. As expected, a dramatic increase in the number of GFP cells present in the skin was observed (Fig. 2). To study the immune response of ZnO NPs, a combination of TPL and SHG was utilized to provide enhanced contrast of ZnO NPs relative to autofluorescence and SHG background in the skin (Fig. 3). This method takes advantage of the unique optical properties of ZnO NPs and can be used to track the long term fate of these particles *in vivo* following exposure.

In vivo MPM imaging was used to visualize the response of the skin following the application of ZnO NPs. Topical exposure of the NPs to the skin did not result in any observable increase in the presence of the GFP cells, suggesting that no inflammatory response due to the exposure had occurred (Fig. 4). In comparison, the positive control experiments with LPS resulted in a dramatic increase in GFP signal 24 hours following exposure. ZnO NP signal was noticeably increased following exposure but then decreased significantly by 48 hours. This suggests that the particles did not penetrate the outer layers of the skin and were eventually removed from the skin. This was expected as several studies have shown that topically-applied ZnO NPs generally do not penetrate through the stratum corneum of intact skin. However, the potential for deeper penetration of these particles is possible in situations where the barrier function of the skin is disrupted.

In the dermal exposure of ZnO NPs, no significant increase in GFP signal was observed suggesting that even if these NPs penetrate the skin they will not cause a significant inflammatory response. A weak increase in the GFP signal was observed in both the dermal exposure study and the corresponding control study by 48 hours. However, due to its late appearance, this signal was attributed to strong autofluorescence from the wound site and not due to an influx of GFP cells caused by an inflammatory response. This can be further be justified by quantifying the increase in the level of GFP signal compared to the LPS exposure positive control treatment. The lack of cellular features in Fig. 6(b) and 6(c), compared to Fig. 6(d), further supports that the increase in GFP signal seen in the ZnO dermal exposure and the control treatment is not due to an inflammatory response, but instead to strong autofluorescence background, likely from proteins within the wound bed. The lack of cellular response in the control incision indicates that the incisions inflicted in these studies alone do not cause a significant immune response. Thus, these results suggests that the ZnO particles did not interact significantly with BM-derived immune cells and did not cause an inflammatory reaction, even when directly applied to the dermis.

In this study, time-lapse imaging of ZnO NPs and GFP cell dynamics was performed for both topical application and dermal exposure. Neither situation resulted in a significant increase in the number of BM-derived cells when compared to a positive control treatment based on LPS. These results suggest that the ZnO NPs used in this study do not have a significant impact on the immune system *in vivo* under the conditions tested, as no obvious immune response is visualized. Future studies are needed to validate the imaging results using histological methods.

ZnO NPs can be manufactured with a wide range of sizes and be coated with various materials. Therefore, future studies are also needed to test whether such parameters can influence immune responses. In particular, emphasis should be placed on the specific ZnO NPs used in commercial sunscreens. Finally, studies are needed to understand the role of ultraviolet exposure on the toxicity of ZnO NPs in the skin. The methods and results in this

#192235 - $15.00 USD Received 14 Jun 2013; revised 9 Aug 2013; accepted 11 Aug 2013; published 29 Aug 2013
(C) 2013 OSA

paper represent a novel approach for tracking the interactions of NPs *in vivo* and for visualizing the cellular response of the exposed tissue. Future toxicology studies based on these methods have great potential for improving our understanding of the interactions of nanoparticles with *in vivo* tissue environments.

Acknowledgments

We gratefully acknowledge Darold Spillman for providing administrative and information technology support related to this research. This research was supported in part by grants from the National Science Foundation (CBET 08-52658 ARRA and CBET 10-33906, S.A.B.). B.W.G. was supported by the Predoctoral National Institutes of Health Environmental Health Sciences Training Program in Endocrine, Developmental, and Reproductive Toxicology at the University of Illinois at Urbana-Champaign. M.D. was supported by a CIHR Canada Graduate Scholarship. Additional information can be found at http://biophotonics.illinois.edu.

#192235 - $15.00 USD Received 14 Jun 2013; revised 9 Aug 2013; accepted 11 Aug 2013; published 29 Aug 2013
(C) 2013 OSA